Sensitivity of Photoelectron Angular Distributions to Molecular Conformations of Anions

*Cate S. Anstöter, Charlie R. Dean, Jan R. R. Verlet**

Department of Chemistry, Durham University, DH1 3LE, United Kingdom

ABSTRACT: An anion photoelectron imaging study probing the sensitivity of the photoelectron angular distribution (PAD) to conformational changes is presented. The PADs of a series of para-substituted phenolate anions is compared with those calculated using the Dyson orbital formalization. Good agreement was attained for the two observed direct detachment channels of all anions, except for the lowest energy detachment channel of para-ethyl phenolate for which two conformations exist that yield very different PADs. The conformational freedom leads to an observed PAD that is the incoherent sum of the PADs from all conformers populated under experimental conditions. In contrast, a second detachment channel shows no sensitivity to the conformational flexibility of para-ethyl phenolate. Our results show that PADs can provide detailed information about the electronic structure of the anion and its conformations.

TOC GRAPHICS

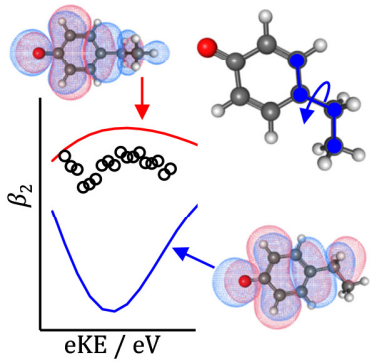

Molecular conformation plays a key role in determining chemical reactivity or biomolecular function and structure. The measurement and understanding of intrinsic interactions that lead to specific conformations represents an important branch of physical chemistry, which impacts many branches of science. The development of new methods that can probe conformations and conformational change may provide new insights. Gas-phase ion spectroscopy in particular has provided a wealth of insight into the intrinsic interactions leading to specific conformations in biological, chemical and catalytic contexts.[1–7] Electronic structure is of course closely linked to molecular structure and, generally, specific geometric structures can have very different electronic structures that in turn lead to differing physical or chemical properties. Anion photoelectron (PE) spectroscopy is a powerful and well-established method that probes electronic structure directly and, by comparison with calculations and vibrational analysis of the Franck-Condon profiles of the PE spectra, can also probe geometric structure.[8–11] Many experimental implementations of PE spectroscopy also measure the photoelectron angular distribution (PAD); here we consider how sensitive these PADs are to geometric changes in a molecular anion.

In principle, the angular component of the PE provides complimentary information to its electron kinetic energy (eKE) spectrum, as it is sensitive to the orbital from which the electron was removed.[12] The PAD is generally quantified by a single anisotropy parameter, β_2, defined for a single photon process as;[13]

$$I(\theta) \propto 1 + \beta_2 P_2(\cos\theta), \tag{1.1}$$

where $P_2(\cos\theta) = \frac{1}{2}(3\cos^2\theta - 1)$ is the second order Legendre polynomial and θ is the angle between the outgoing electron vector and the polarization axis of the excitation field, $\boldsymbol{\varepsilon}$. The two

limiting values of β_2 are +2 and –1, corresponding to emission predominantly parallel ($\cos^2\theta$ distribution) and perpendicular ($\sin^2\theta$ distribution) to $\boldsymbol{\varepsilon}$, respectively. A negative β_2 is broadly attributed to photodetachment from an orbital with p- or π-character, whereas a positive sign corresponds to s- or σ-character,[14] although its value depends sensitively on the interference between all possible outgoing partial waves. Generally, at low eKE, symmetry arguments can provide qualitative insight into the nature of the molecular orbital from which the electron is removed.[14] More recently, semi-quantitative approaches to predicting β_2 parameters have been developed[15,16] and applied to photodetachment[17–19] and scattering processes in water clusters.[20]

One computational approach, based on electronic structure calculations, that has emerged as a useful means of computing the PADs from anions is based on the use of Dyson orbitals, most commonly through implementation of the equation-of-motion coupled-cluster (EOM-CCSD) formalization.[16,21,22] Dyson orbitals can be thought of as the one electron wavefunction of the leaving electron, before photodetachment.[23–26] For anionic systems, the Dyson orbital, $\psi_{\text{Dyson}}(1)$, represents the overlap between an N electron molecular wavefunction and the N^{-1} electron wavefunction of the corresponding anion:

$$\psi_{\text{Dyson}}(1) = \sqrt{N}\int \Psi_i^N(1,...,n)\Psi_f^{N-1}(2,...,n)d2...dn\,, \tag{1.2}$$

where i and f are the initial and final states, respectively (the anion and neutral state in the present context). As such, the molecular orbital (MO) from which the electron is removed provides a good approximation of the Dyson orbital. The PADs can be predicted by computing the transition dipole moments between the Dyson orbital and a free electron, with appropriate averaging of the molecular frame.[16,27] In the present paper, we explore the sensitivity of the PADs to changes in molecular structure that might be considered to have small effects on the

electronic structure. The sensitivity of PADs to *gauche* and *anti* conformers of neutral species has previously been noted and was used to assign PE spectral bands.[28] Here, we performed a combined PE imaging and computational study on a series of para-substituted phenolate anions shown in Figure 1: para-methyl phenolate (pMP^-), para-ethyl phenolate (pEP^-), and para-vinyl phenolate (pVP^-). These three phenolate anions have similar structures, which may in turn be expected to have broadly similar electronic structure.

Figure 1 shows the PE images and spectra of the three phenolate anions at the two photon energies $h\nu$ = 2.85 and 4.00 eV. The PE spectra at $h\nu$ = 2.85 eV show a single direct detachment feature, while the $h\nu$ = 4.00 eV shows an additional higher binding energy peak. These spectra are consistent with previous measurements on phenolate anions by the Lineberger group, albeit at lower resolution.[29,30] The highest eKE feature corresponds to photodetachment from the ground state of the anion to the ground state of the neutral, $S_0 + h\nu \rightarrow D_0 + e^-$. The peak at lower eKE that is only visible at $h\nu$ = 4.00 eV corresponds to the $S_0 + h\nu \rightarrow D_1 + e^-$ detachment channel in which the neutral is formed in its first excited state. In the following, we will refer to these two photodetachment processes as the D_0 or the D_1 detachment channel, respectively.

The experimental PADs of both detachment channels were quantified using the β_2 parameter (Equation 1.1). The PADs were determined from a series of PE images taken over a range of photon energies with 50 meV intervals. The β_2 values across the highest intensity of the peaks were averaged and plotted as a function of eKE above the threshold of each channel. The measured β_2 parameters for the D_0 and D_1 detachment channel covering a range of nearly 1 eV in eKE are plotted in Figure 2 and 3, respectively. The error associated with the β_2 values is on the order of ±0.1. Also shown in Figures 2 and 3 are the calculated β_2 parameters including the

relevant Dyson orbital corresponding to the detachment channel. For pEP^-, two β_2 parameters were calculated (Figure 2(b)), corresponding to different conformers. The eKE range over which β_2 was measured has been restricted because of the presence of electronic resonances. Resonances have been shown to cause changes in the PE spectra of both pMP^- and the phenolate anion[29,30] and many other molecular anions, as well as in PADs.[19,31–33] PADs from resonances are not accounted for within the current calculations.

For the D_1 detachment channel, the computed PADs are in very good agreement with those experimentally observed (Figure 3). For the three phenolate anions, the PAD is characterized by a negative β_2 value. Previous studies have confirmed the nature of the D_1 state,[30,34] which is in good agreement with the experimental onset observed here and our electronic structure calculations. The Dyson orbitals corresponding to the D_1 detachment channel for pMP^-, pEP^-, and pVP^- are shown in Figure 3(a), (b), and (c), respectively. These show that the electron density is primarily localized to the phenolate-motif in all molecules. The dominant character of this Dyson orbital is a lone pair of the oxygen atom (p-character), which qualitatively agrees with the experimentally observed negative β_2 values. The convergence of $\beta_2 \rightarrow 0$ as eKE $\rightarrow 0$ arises from the Wigner law,[35] which dictates the predominance of $l = 0$ partial waves to the total outgoing electron near threshold.

The D_0 detachment channels for pMP^- and pVP^- have negative experimental β_2 values and vary more rapidly with eKE compared to the D_1 channel as shown in Figure 2(a) and (c), respectively. For these two anions, there is again very good agreement with the calculated PADs. Qualitatively, a negative value of β_2 is indicative of p- or π-character of the MO from which the electron is detached, which is consistent with the calculated Dyson orbitals for the D_0 detachment channel (See Figure 2). For pEP^-, β_2 is observed to be broadly isotropic with a value

close to 0. At first glance, the striking difference between the PADs of pEP^- and pMP^- or pVP^- is surprising. Firstly, one might envisage a larger change in electronic structure between pVP^- and the other two because of the increased conjugation. Secondly, similar differences are not seen for the D_1 detachment channel. Indeed, the calculated PADs for pEP^- with a similar planar geometry as for pMP^- and pVP^- indicates that a negative PAD is expected for this too (see Figure 2(b)). However, pEP^- has greater conformational flexibility than pMP^- and pVP^-, due to the saturated ethyl chain. A second conformation was found to be the global minimum energy structure, related by torsion about a single bond as shown in Figure 4. The calculated PAD of the lowest energy conformer is dramatically different, showing an inversion of sign with respect to all other calculated PADs in this energy range. This observation is more consistent with the experimentally observed anisotropy, although not quantitatively correct.

A relaxed potential energy scan as a function of the torsion angle to the ethyl-chain is shown in Figure 4(a). The out-of-plane structure is the lowest energy with a 70 meV (565 cm^{-1}) barrier to the planar conformation. The torsional mode connecting the two geometries can be readily identified from the calculations (see Figure 4(b)) and the (harmonic) frequency of the mode is 56.4 cm^{-1} in the out-of-plane geometry (64.7 cm^{-1} for the planar geometry). Hence, the zero-point energy associated with this torsion is approximately 30 cm^{-1} (~3.5 meV). In principle, the wavefunctions of the torsional levels can be calculated[36] from this potential. The square of these wavefunctions then provides a distribution of possible conformations and the PADs for these conformations can be calculated from their Dyson orbitals. If the PAD of each conformation is correctly represented, then the weighted sum of these PADs can be used to reproduce the experimentally observed PAD. However, the present experiments were conducted with ions thermalized in a ~300 K ion trap. Although only a small fraction (<10%) of the

molecules have energies above the barrier, it is clear that on average, several quanta of energy are imparted in the torsional mode at 300 K. Hence, to quantitatively determine the conformational distribution would require a precise knowledge of the temperature and a high quality potential energy surface for the torsion based on spectroscopic data which is not available. Nevertheless, as most of the pEP^- molecules are at energies well below the barrier, the out-of-plane conformation will have the highest probability and therefore, qualitatively, we expect the overall PAD to predominantly represent that of the lowest-energy conformation in agreement with our observations. The use of temperature controlled cryogenic ion traps coupled with PE imaging[37,38] would allow the molecules to be cooled so that only the lowest modes are populated which would greatly simplify a quantitative analysis.

Based on the above discussion, the rigidity of the molecules impacts the observed PADs. The most rigid of the three anions studied is pVP^-. At elevated temperatures, the distribution of the Dyson orbital can be considered to be static and pVP^- shows the closest agreement between experimental and predicted PADs. For pMP^-, good agreement between experimental and computational results are seen, however, the experimental values are generally less negative than the predicted ones. For pMP^- at finite temperature, the methyl-group will have rotational freedom and such motion may have small, but important effects on the Dyson orbital. A similar point was noted in a recent photodetachment study on tocopherol anions,[39] which have similar Dyson orbitals as the D_0 channel in this study. The PADs were mostly isotropic except for δ-tocopherol in which the ring contains only H atoms in the ortho- and meta-positions. The other tocopherols have methyl groups in these positions that either lower the symmetry of the Dyson orbital, or in the case of α-tocopherol, may reduce the PAD anisotropy through rotational freedom. Overall, however, rotamers are likely to have a much smaller effect on PADs than

conformers, which is consistent with our observations for pMP^- (Figure 2(a)). The flexibility in the ethyl-chain in pEP^- yields two distinct conformers, for which the electron distribution of the MOs have some distinctive differences. The planar, higher energy, conformer has a Dyson orbital with the same nodal character as pMP^- and pVP^- and as a result, the predicted PADs are very similar for the three molecules (see Figure 2). When the ethyl-chain in pEP^- is bent out of the plane of the phenolate ring, its Dyson orbital shows an increase in the number of nodes. It appears that this change in MO character causes the drastic change in PAD, illustrating how sensitive the PADs are to such small changes in electronic structure caused by conformational flexibility.

The sensitivity of PADs to conformation is starkly different for the two detachment channels. The D_1 channel shows no sensitivity to the conformational flexibility of pEP^-. Using similar arguments as used for the D_0 detachment channel, this may be rationalized by the lack of electron density in the Dyson orbital on the ethyl-chain. Calculations show that the PADs are almost identical for both pEP^- isomers in the energy range shown here. The small additional Dyson orbital density on the vinyl chain of pVP^- observed for the D_1 channel also does not appear to have altered the expected PADs significantly compared to pMP^- and pEP^-, because the overall nodal structure of the Dyson orbital remains unchanged.

In summary, we have shown through a series of PE imaging studies of para-substituted phenolate anions that conformation can subtly alter the electronic structure of certain MOs. PADs can be extremely sensitive to these changes, which can be probed directly through PE imaging. Computation of the Dyson orbital corresponding to specific photodetachment channels allows the PADs to be predicted and compared with experiment and shows very good overall agreement. Hence, by combining experiment and theory, the dominant conformation under

experimental conditions can be determined through the PADs. Moreover, the sensitivity of the PAD to the Dyson orbital provides detailed information concerning the electronic structure of the anion. Finally, the sensitivity of the PADs to conformation may also be informative for dynamical processes in which time-resolved photoelectron imaging could track large amplitude motions of complex molecules through real-time changes in the PADs.

METHODOLOGY

The experimental set-up has been detailed in full elsewhere.[19,40] Briefly, deprotonated anions were produced by electrospray ionization (ESI) of ~1 mM solutions of p-cresol and 4-ethyl-phenol in methanol. The ESI source was coupled to the first of several vacuum regions by a transfer capillary. Anions progressed along a sequence of ring-electrode ion guides, consisting of radially-confining RF and longitudinal DC ramps. At the end of the ion guides was an ion trap, which pulsed a packet of anions into a collinear Wiley-McLaren time-of-flight mass spectrometer.[41] Mass-selected ion packets were then sent into in a velocity map PE imaging spectrometer,[42,43] where they were irradiated by a tunable ~6 ns laser pulse from a Nd:YAG pumped optical parametric oscillator (Continuum Surelite II-10, Horizon I) . Raw PE images were analyzed using the Polar Onion Peeling (POP) algorithm[44] to determine both the PE spectrum and the PAD. PE spectra were calibrated from the atomic I^- spectrum and have a resolution of ~5%.

Deprotonated anions of pVP were produced from a ~1 mM solution of para-coumaric acid (pCA) in methanol with a few drops of NH_3 added, site-specifically deprotonating at the phenolate group. The pCA anion underwent collisional induced dissociation to lose CO_2 and form pVP^- in the ion guide ,which were then rethermalized and mass-selected.[19]

Initial density functional theory (DFT) calculations were used to optimize the geometries of the ground states of the neutral and anion using the QChem 4.4 package.[45] Geometries were confirmed to be energetic minima by vibrational frequency analysis. A relaxed potential energy surface scan was performed along torsion about the ethyl-chain with respect to the phenolate plane (see Figure 4(a)). All DFT calculations used the B3LYP functional[46–49] and the aug-cc-pVDZ Dunning basis set.[50] Additional time-dependent DFT calculations, using the Tamm-Dancoff approximation,[51] confirmed the energetics and character of the excited state of the neutral accessed experimentally. Using the same basis set as DFT calculations, the geometries of all anions were then optimized using CCSD and EOM-IP-CCSD calculations of the Dyson orbitals were performed. The initial reference wavefunction, $\Psi_i^N(1,...,n)$, is that of the anion ground state and is the same for both D_0 and D_1 detachment channels. The final wavefunction, $\Psi_f^{N-1}(2,...,n)$, is that of the ground and first excited state of the neutral for the D_0 and D_1 detachment channels, respectively. The PAD for both direct detachment channels were calculated using the ezDyson program (version 3.2) developed by Krylov and coworkers.[52]

AUTHOR INFORMATION

*Corresponding Author: j.r.r.verlet@durham.ac.uk. The authors declare no competing financial interests.

ACKNOWLEDGMENT

We thank Eckart Wrede and David Tozer for useful discussions about internal rotation of molecules. This work was funded by the ERC (Starting Grant 306536).

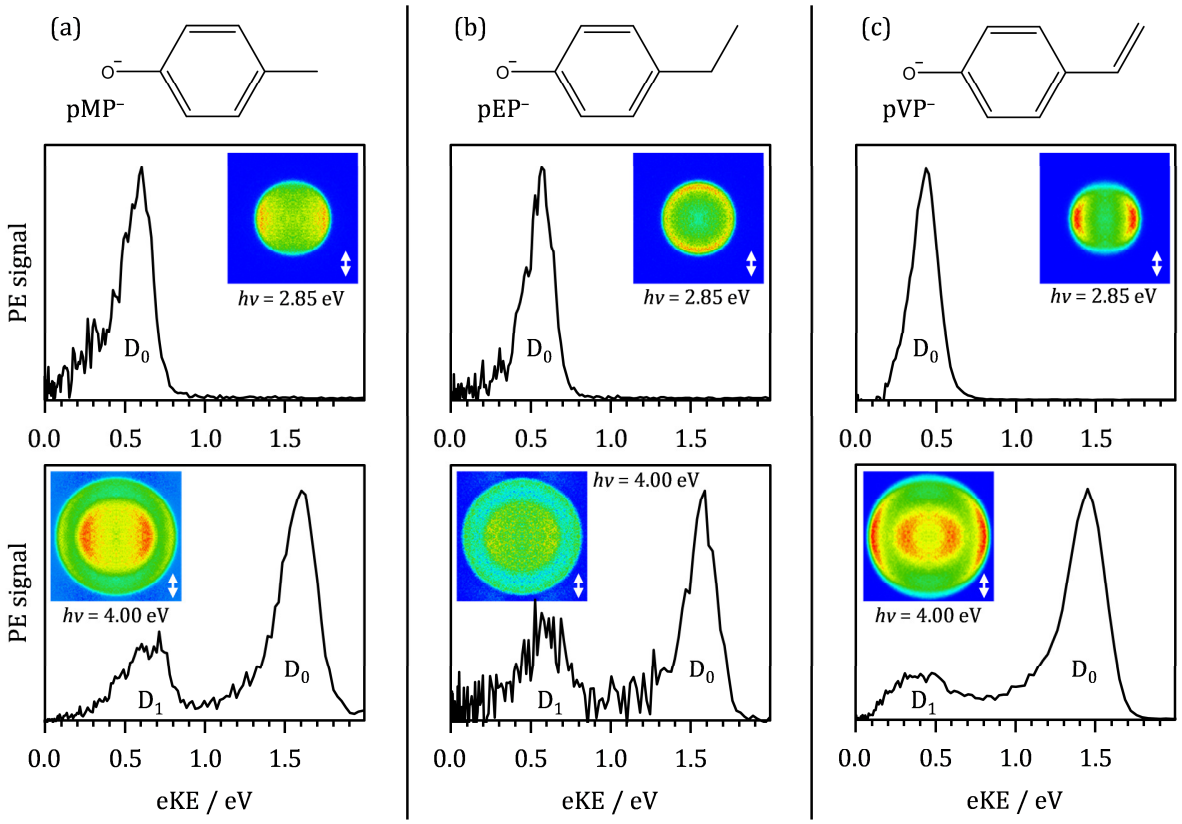

Figure 1. Photoelectron spectra acquired at photon energies of 2.85 and 4.00 eV for (a) pMP–, (b) pEP–, and (c) pVP–. Respective raw images are inset with the polarization axis of the laser shown by the double arrow.

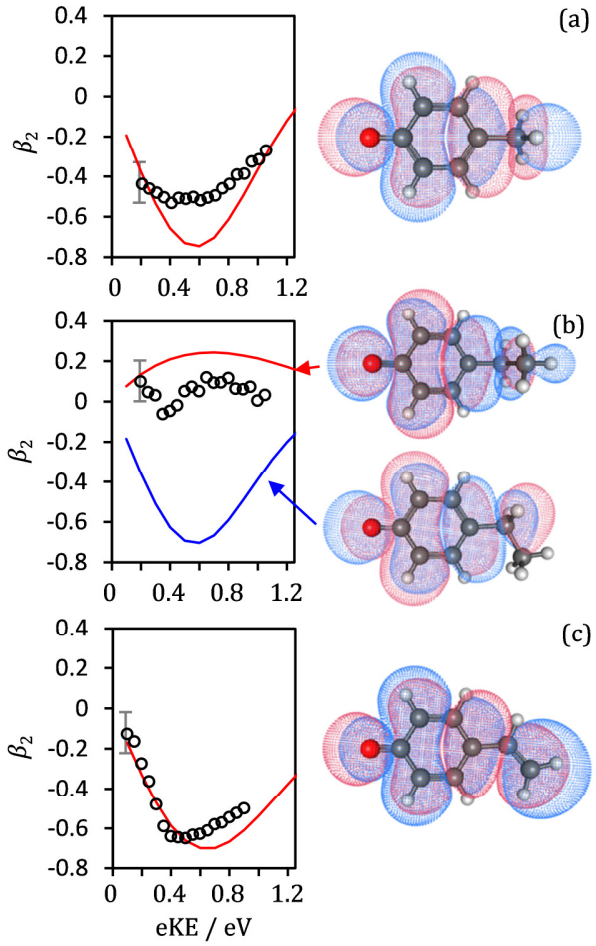

Figure 2. Plots of the experimental (circles) and computed (solid lines) β_2 parameters as a function of eKE for the D_0 detachment channel for (a) pMP^-, (b) pEP^- and (c) pVP^-. For pEP^- two computed PADs are shown corresponding to global (red) and local (blue) minimum energy structures. The right hand side shows the relevant Dyson orbitals.

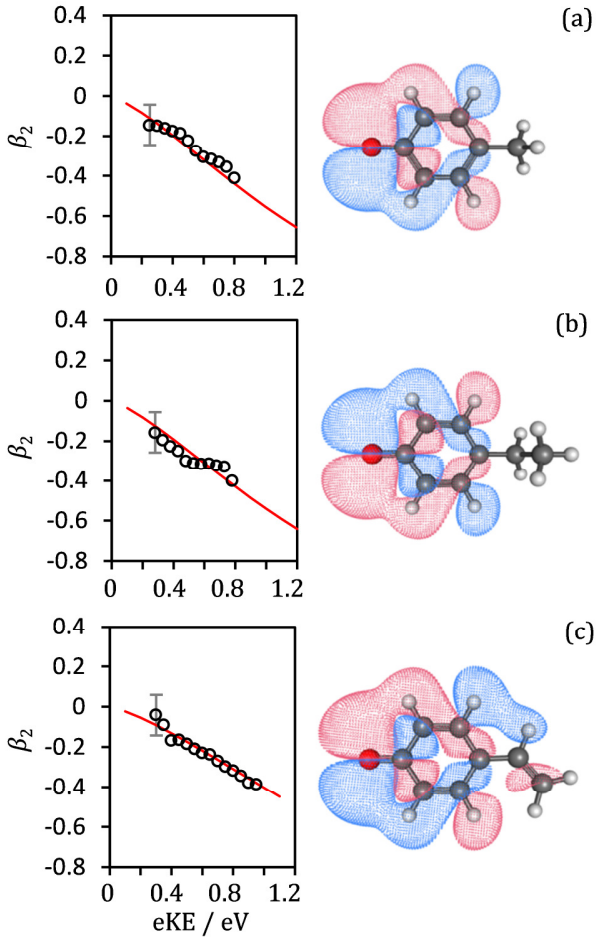

Figure 3. Plots of the experimental (circles) and computed (solid lines) β_2 parameters for (a) pMP^-, (b) pEP^- and (c) pVP^-, as a function of eKE for the D_1 detachment feature. The right hand side shows the relevant Dyson orbitals.

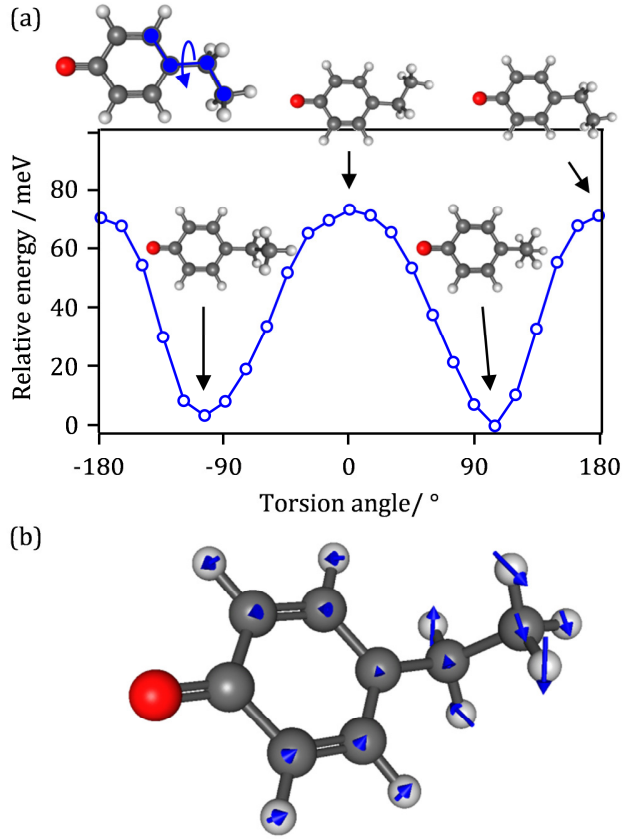

Figure 4. (a) A relaxed potential energy scan of pEP^- as a function of the torsion angle around the ethyl chain as shown. Above and below are shown snapshots of conformations where the ethyl-chain is in the plane and out of the plane of the phenolate, respectively. (b) Calculated torsional mode for pEP^- indicating the displacement vectors of the atoms.

REFERENCES

(1) Park, S. T.; Kim, S. K.; Kim, M. S. Observation of Conformation-Specific Pathways in the Photodissociation of 1-Iodopropane Ions. *Nature* **2002**, *415*, 306–308.

(2) Rizzo, T. R.; Stearns, J. A.; Boyarkin, O. V. Spectroscopic Studies of Cold, Gas-Phase Biomolecular Ions. *Int. Rev. Phys. Chem.* **2009**, *28*, 481–515.

(3) Wolk, A. B.; Leavitt, C. M.; Garand, E.; Johnson, M. A. Cryogenic Ion Chemistry and Spectroscopy. *Acc. Chem. Res.* **2014**, *47*, 202–210.

(4) Brøndsted Nielsen, S.; Dedonder, C.; Féraud, G.; Jouvet, C. *Photophysics of Ionic Biochromophores*; Brøndsted Nielsen, S., Wyer, J. A., Eds.; Physical Chemistry in Action; Springer Berlin Heidelberg: Berlin, Heidelberg, 2013.

(5) Garand, E.; Kamrath, M. Z.; Jordan, P. A.; Wolk, A. B.; Leavitt, C. M.; McCoy, A. B.; Miller, S. J.; Johnson, M. A. Determination of Noncovalent Docking by Infrared Spectroscopy of Cold Gas-Phase Complexes. *Science* **2012**, *335*, 694–698.

(6) *Gas-Phase IR Spectroscopy and Structure of Biological Molecules*, 1st ed.; Rijs, A. M., Oomens, J., Eds.; Topics in Current Chemistry; Springer International Publishing, 2015; Vol. 364.

(7) Duffy, E. M.; Marsh, B. M.; Voss, J. M.; Garand, E. Characterization of the Oxygen Binding Motif in a Ruthenium Water Oxidation Catalyst by Vibrational Spectroscopy. *Angew. Chemie Int. Ed.* **2016**, *55*, 4079–4082.

(8) Lineberger, W. C. Once upon Anion: A Tale of Photodetachment. *Annu. Rev. Phys. Chem.*

2013, *64*, 21–36.

(9) Stokes, S. T.; Li, X.; Grubisic, A.; Ko, Y. J.; Bowen, K. H. Intrinsic Electrophilic Properties of Nucleosides: Photoelectron Spectroscopy of Their Parent Anions. *J. Chem. Phys.* **2007**, *127*, 84321.

(10) Mabbs, R.; Grumbling, E. R.; Pichugin, K.; Sanov, A. Photoelectron Imaging: An Experimental Window into Electronic Structure. *Chem. Soc. Rev.* **2009**, *38*, 2169–2177.

(11) Neumark, D. M. Slow Electron Velocity-Map Imaging of Negative Ions: Applications to Spectroscopy and Dynamics. *J. Phys. Chem. A* **2008**, *112*, 13287–13301.

(12) Reid, K. L. Photoelectron Angular Distributions. *Annu. Rev. Phys. Chem.* **2003**, *54*, 397–424.

(13) Cooper, J.; Zare, R. N. Angular Distribution of Photoelectrons. *J. Chem. Phys.* **1968**, *48*, 942–943.

(14) Sanov, A. Laboratory-Frame Photoelectron Angular Distributions in Anion Photodetachment: Insight into Electronic Structure and Intermolecular Interactions. *Annu. Rev. Phys. Chem.* **2014**, *65*, 341–363.

(15) Khuseynov, D.; Blackstone, C. C.; Culberson, L. M.; Sanov, A. Photoelectron Angular Distributions for States of Any Mixed Character: An Experiment-Friendly Model for Atomic, Molecular, and Cluster Anions. *J. Chem. Phys.* **2014**, *141*, 124312.

(16) Oana, C. M.; Krylov, A. I. Cross Sections and Photoelectron Angular Distributions in Photodetachment from Negative Ions Using Equation-of-Motion Coupled-Cluster Dyson

Orbitals. *J. Chem. Phys.* **2009**, *131*, 124114.

(17) Jagau, T. C.; Dao, D. B.; Holtgrewe, N. S.; Krylov, A. I.; Mabbs, R. Same but Different: Dipole-Stabilized Shape Resonances in CuF^- and AgF^-. *J. Phys. Chem. Lett.* **2015**, *6*, 2786–2793.

(18) Culberson, L. M.; Blackstone, C. C.; Wallace, A. A.; Sanov, A. Aromatic Stabilization and Hybridization Trends in Photoelectron Imaging of Heterocyclic Radicals and Anions. *J. Phys. Chem. A* **2015**, *119*, 9770–9777.

(19) Stanley, L. H.; Anstöter, C. S.; Verlet, J. R. R. Resonances of the Anthracenyl Anion Probed by Frequency-Resolved Photoelectron Imaging of Collision-Induced Dissociated Anthracene Carboxylic Acid. *Chem. Sci.* **2017**, *8*, 3054–3061.

(20) Hartweg, S.; Yoder, B. L.; Garcia, G. A.; Nahon, L.; Signorell, R. Size-Resolved Photoelectron Anisotropy of Gas Phase Water Clusters and Predictions for Liquid Water. *Phys. Rev. Lett.* **2017**, *118*, 103402.

(21) Melania Oana, C.; Krylov, A. I. Dyson Orbitals for Ionization from the Ground and Electronically Excited States within Equation-of-Motion Coupled-Cluster Formalism: Theory, Implementation, and Examples. *J. Chem. Phys.* **2007**, *127*, 234106.

(22) Jagau, T.-C.; Krylov, A. I. Characterizing Metastable States beyond Energies and Lifetimes: Dyson Orbitals and Transition Dipole Moments. *J. Chem. Phys.* **2016**, *144*, 54113.

(23) Pickup, B. T. On the Theory of Fast Photoionization Processes. *Chem. Phys.* **1977**, *19*,

193–208.

(24) McWeeny, R.; Pickup, B. T. Quantum Theory of Molecular Electronic Structure. *Reports Prog. Phys.* **1980**, *43*, 1065–1144.

(25) Deleuze, M.; Pickup, B. T.; Delhalle, J. Plane Wave and Orthogonalized Plane Wave Many-Body Green's Function Calculations of Photoionization Intensities. *Mol. Phys.* **1994**, *83*, 655–686.

(26) Seabra, G. M.; Kaplan, I. G.; Zakrzewski, V. G.; Ortiz, J. V. Electron Propagator Theory Calculations of Molecular Photoionization Cross Sections: The First-Row Hydrides. *J. Chem. Phys.* **2004**, *121*, 4143–4155.

(27) Dill, D. Fixed-Molecule Photoelectron Angular Distributions. *J. Chem. Phys.* **1976**, *65*, 1130–1133.

(28) Utsunomiya, C.; Kobayashi, T.; Nagakura, S. Photoelectron Angular Distribution Measurements for Some Aliphatic Alcohols, Amines and Halides. *Bull. Chem. Soc. Jpn.* **1980**, *53*, 1216–1220.

(29) Nelson, D. J.; Gichuhi, W. K.; Miller, E. M.; Lehman, J. H.; Lineberger, W. C. Anion Photoelectron Spectroscopy of Deprotonated *Ortho* -, *Meta* -, and *Para* -Methylphenol. *J. Chem. Phys.* **2017**, *146*, 74302.

(30) Gunion, R. F.; Gilles, M. K.; Polak, M. L.; Lineberger, W. C. Ultraviolet Photoelectron Spectroscopy of the Phenide, Benzyl and Phenoxide Anions, with Ab Initio Calculations. *Int. J. Mass Spectrom. Ion Process.* **1992**, *117*, 601–620.

(31) Anstöter, C. S.; Bull, J. N.; Verlet, J. R. R. Ultrafast Dynamics of Temporary Anions Probed through the Prism of Photodetachment. *Int. Rev. Phys. Chem.* **2016**, *35*, 509–538.

(32) West, C. W.; Bull, J. N.; Hudson, A. S.; Cobb, S. L.; Verlet, J. R. R. Excited State Dynamics of the Isolated Green Fluorescent Protein Chromophore Anion Following UV Excitation. *J. Phys. Chem. B* **2015**, *119*, 3982–3987.

(33) West, C. W.; Bull, J. N.; Antonkov, E.; Verlet, J. R. R. Anion Resonances of Para-Benzoquinone Probed by Frequency-Resolved Photoelectron Imaging. *J. Phys. Chem. A* **2014**, *118*, 11346–11354.

(34) Cheng, C.-W.; Witek, H.; Lee, Y.-P. Rovibronic Bands of the $\tilde{A}^2B_2 \leftarrow \tilde{X}^2B_1$ Transition of C_6H_5O and C_6D_5O Detected with Cavity Ringdown Absorption near 1.2 Mm. *J. Chem. Phys.* **2008**, *129*, 154307.

(35) Wigner, E. P. On the Behavior of Cross Sections Near Thresholds. *Phys. Rev.* **1948**, *73* (9), 1002–1009.

(36) Lewis, J. D.; Malloy, T. B.; Chao, T. H.; Laane, J. Periodic Potential Functions for Pseudorotation and Internal Rotation. *J. Mol. Struct.* **1972**, *12*, 427–449.

(37) Wang, L.-S. Perspective: Electrospray Photoelectron Spectroscopy: From Multiply-Charged Anions to Ultracold Anions. *J. Chem. Phys.* **2015**, *143*, 40901.

(38) Wang, X.-B. Cluster Model Studies of Anion and Molecular Specificities via Electrospray Ionization Photoelectron Spectroscopy. *J. Phys. Chem. A* **2017**, *121*, 1389–1401.

(39) Anstöter, C. S.; West, C. W.; Bull, J. N.; Verlet, J. R. R. The Vitamin E Radical Probed by

Anion Photoelectron Imaging. *J. Phys. Chem. B* **2016**, *120*, 7108–7113.

(40) Lecointre, J.; Roberts, G. M.; Horke, D. A.; Verlet, J. R. R. Ultrafast Relaxation Dynamics Observed through Time-Resolved Photoelectron Angular Distributions. *J. Phys. Chem. A* **2010**, *114*, 11216–11224.

(41) Wiley, W. C.; McLaren, I. H. Time-of-Flight Mass Spectrometer with Improved Resolution. *Rev. Sci. Instrum.* **1955**, *26*, 1150–1157.

(42) Horke, D. A.; Roberts, G. M.; Lecointre, J.; Verlet, J. R. R. Velocity-Map Imaging at Low Extraction Fields. *Rev. Sci. Instrum.* **2012**, *83*, 63101.

(43) Eppink, A. T. J. B.; Parker, D. H. Velocity Map Imaging of Ions and Electrons Using Electrostatic Lenses: Application in Photoelectron and Photofragment Ion Imaging of Molecular Oxygen. *Rev. Sci. Instrum.* **1997**, *68*, 3477–3484.

(44) Roberts, G. M.; Nixon, J. L.; Lecointre, J.; Wrede, E.; Verlet, J. R. R. Toward Real-Time Charged-Particle Image Reconstruction Using Polar Onion-Peeling. *Rev. Sci. Instrum.* **2009**, *80*, 53104.

(45) Shao, Y.; Gan, Z.; Epifanovsky, E.; Gilbert, A. T. B.; Wormit, M.; Kussmann, J.; Lange, A. W.; Behn, A.; Deng, J.; Feng, X.; et al. Advances in Molecular Quantum Chemistry Contained in the Q-Chem 4 Program Package. *Mol. Phys.* **2015**, *113*, 184–215.

(46) Vosko, S. H.; Wilk, L.; Nusair, M. Accurate Spin-Dependent Electron Liquid Correlation Energies for Local Spin Density Calculations: A Critical Analysis. *Can. J. Phys.* **1980**, *58*, 1200–1211.

(47) Lee, C.; Yang, W.; Parr, R. G. Development of the Colle-Salvetti Correlation-Energy Formula into a Functional of the Electron Density. *Phys. Rev. B* **1988**, *37*, 785–789.

(48) Becke, A. D. Density-Functional Thermochemistry. III. The Role of Exact Exchange. *J. Chem. Phys.* **1993**, *98*, 5648–5652.

(49) Stephens, P. J.; Devlin, F. J.; Chabalowski, C. F.; Frisch, M. J. Ab Initio Calculation of Vibrational Absorption and Circular Dichroism Spectra Using Density Functional Force Fields. *J. Phys. Chem.* **1994**, *98*, 11623–11627.

(50) Dunning, T. H. Gaussian Basis Sets for Use in Correlated Molecular Calculations. I. The Atoms Boron through Neon and Hydrogen. *J. Chem. Phys.* **1989**, *90*, 1007–1023.

(51) Hirata, S.; Head-Gordon, M. Time-Dependent Density Functional Theory within the Tamm–Dancoff Approximation. *Chem. Phys. Lett.* **1999**, *314*, 291–299.

(52) Gozem, S.; Krylov, A. I. ezDyson. 2016.